2024 European Control Conference (ECC)
June 25-28, 2024. Stockholm, Sweden

3D Directed Formation Control with Global Shape Convergence using Bispherical Coordinates

Omid Mirzaeedodangeh, Farhad Mehdifar, and Dimos V. Dimarogonas

Abstract— **In this paper, we present a novel 3D formation control scheme for directed graphs in a leader-follower multi-agent setup,, achieving (almost) global convergence to the desired shape. Specifically, we introduce three controlled variables representing bispherical coordinates that uniquely describe the formation in 3D. Acyclic triangulated directed graphs (a class of minimally acyclic persistent graphs) are used to model the inter-agent sensing topology, while the agents' dynamics are governed by single-integrator model. Our analysis demonstrates that the proposed decentralized formation controller ensures (almost) global asymptotic stability while avoiding potential shape ambiguities in the final formation. Furthermore, the control laws are implementable in arbitrarily oriented local coordinate frames of follower agents using only low-cost onboard vision sensors, making it suitable for practical applications. Finally, we validate our formation control approach by a simulation study.**

I. Introduction

Formation control in multiagent systems has undergone extensive investigation over the past decade. Depending on the sensing and controlled variables, previous research efforts can be broadly classified into [1], [2]: position-based , displacement-based, distance-based [3], [4], bearing-based [5], and angle-based [6]–[8] methodologies. Works in [9], [10] provide more recent classifications on formation control methods as well as a comparative literature review on issues related to target formation's constraints, required measurements, and shape convergence.

Within these categories, the position-based approach requires agents to possess a common understanding of a global coordinate system. Conversely, the displacement-based (often referred to as consensus-based) and bearing-based methods require that agents' local coordinate frames are perfectly aligned (have common orientation).

Meanwhile, coordinate-free techniques, namely, distance- and angle-based methods in [3], [4], [6], [7], and [9] present a more attractive architecture for formation control due to their reduced implementation complexities and their ability to characterize the desired formation shape by a set of coordinate-free scalar variables, typically involving distances or angles. These scalar variables serve to define formation errors for the individual agents. Furthermore, agents must possess measurements of vectorized relative information of their neighboring agents (e.g., relative positions or bearings) in their local coordinate frames to constitute a control law.

This work is supported by ERC CoG LEAFHOUND, the KAW foundation, and the Swedish Research Council (VR).

O. Mirzaeedodangeh, F. Mehdifar and D. V. Dimarogonas are with the Division of Decision and Control Systems, KTH Royal Institute of Technology, Stockholm, Sweden. omidm@kth.se; mehdifar@kth.se; dimos@kth.se

Thus, coordinate-free approaches facilitate the design and implementation of formation control laws within the confines of agents' local coordinate frames, obviating the necessity for global position measurements, such as those provided by GPS systems, or the presumption that agents' local coordinate frames are aligned. Another significant benefit of coordinate-free formation control strategies is the cost-effectiveness for agents. This is because they mandate simpler sensing and interaction mechanisms. While a majority of coordinate-free techniques depend on relative position measurements for all agents, only a few existing methods use only bearing or vision-based measurements [7], [9], [11], [7]. Vision based measurements are more practical since bearing data is captured straightforwardly using onboard cameras, making it more advantageous in real-world settings [12].

It is worth noting that the majority of existing research on coordinate-free formation control operates under the assumption of bidirectional sensings. This line of research often relies on various graph rigidity concepts, including distance, angle, ratio-of-distances, and sign rigidity notions [6], [7], [9], [10]. However, from a practical standpoint, it is more realistic to consider directed sensing among agents due to inherent sensing limitations or issues introduced by measurement mismatches in undirected formation control [13]. In this regard, the concept of persistent graphs emerged as the directed counterpart of distance rigidity [14]. Earlier control designs for achieving persistent formations can be found in [4]. Regrettably, most coordinate-free formation control methods offer guarantees of local (non global) convergence to the desired shape. This means that even if agents eventually meet the desired formation constraints, they might not converge to the desired shape due to issues like reflection, flip, and flex ambiguities as highlighted in [3], [6], [7], [9], [10].

To deal with the issue of ambiguous shapes, several recent studies have proposed 2D and 3D distance-based formations by incorporating additional formation constraints to agents, such as signed areas/angles and volumes, to allow defining the target shape uniquely [10], [15]–[19]. However, these approaches inadvertently introduce undesired equilibria at particular agent positions through the control design procedure, which significantly complicates the controllers' gain adjustment for ensuring global shape convergence [15], [16], [17]. Recent studies have introduced an alternative approach to guarantee global convergence of coordinate-free formations. For instance, [20], [21], utilize formation error variables along orthogonal directions to characterize directed 2D and 3D distance-based formations with guaranteed (almost) global convergence to the desired shape, respectively. Furthermore, [8] has provided global stabilization for the angle-rigid formations. However, agents must use relative position information. Moreover, recently [11] proposed a 2D directed formation control approach using orthogonal bipolar coordinate variables to achieve almost global convergence to the desired shape. The main advantages of [11] w.r.t. [20] and [8] are in employing bearing measurements instead of relative position measurements for follower agents and also providing extra degrees of freedom for adjusting scale and orientation of the formation. Nevertheless, the results in [8] and [11] are only limited to 2D formations.

In this work, inspired by [11], we present a 3D directed coordinate-free formation control method using bispherical coordinates. Our method ensures (almost) global convergence to the desired shape while using only vision-based sensing for follower agents. We utilize triangulated acyclic minimally persistent graphs to model the inter-agent sensing topology, which gives rise to a distance-rigid directed leader-follower structure with a minimal number of edges. Moreover, our novel approach utilizes local bispherical coordinates to characterize formation errors, relying on onboard vision sensors for bearing and distance ratio measurements. This technique circumvents the need for relative position measurements, which are often challenging to obtain in environments like deep space. Leveraging the fact that each follower's formation errors can be reduced (independently) by moving along the three orthogonal directions of its associated bishperical coordinate basis, we design decentralized controllers achieving (almost) global asymptotic convergence to the target shape. To the best of the authors' knowledge, this work is the first to employ bispherical coordinates for coordinate-free 3D formation control for achieving (almost) global shape convergence without encountering undesired equilibria.

II. Problem Formulation

Consider a multiagent system composed of n mobile agents in 3D, governed by the following dynamics:

$$\dot{p}_i = u_i, \quad i = 1, \ldots, n, \tag{1}$$

where $p_i \in \mathbb{R}^3$ and $u_i \in \mathbb{R}^3$ are the position and the velocity-level control input of agent i expressed with respect to a global coordinate frame, respectively. Let us model the sensing topology among agents as a directed graph $\mathcal{G} = (\mathcal{V}, \mathcal{E})$, where $\mathcal{V} = \{1, 2, \ldots, n\}$ is the set of vertices representing the agents and $\mathcal{E} = \{(j, i) \mid j, i \in \mathcal{V}, j \neq i\}$, where if $(j, i) \in \mathcal{E} \Rightarrow (i, j) \notin \mathcal{E}$, is the set of directed edges modeling the directed sensing among the agents. To be more precise, $(j, i) \in \mathcal{E}$ denotes an edge that starts from vertex j (source) and sinks at vertex i, and its direction is indicated by $j \to i$. For (j, i), we say i is the neighbor of j. The relative position vector p_{ij}, and the *relative bearing* vector $\hat{v}_{ij} \in \mathbb{R}^3$ corresponding to the directed edge (j, i) are defined as:

$$p_{ji} := p_i - p_j, \quad \hat{v}_{ij} := \frac{p_i - p_j}{\|p_i - p_j\|}, \quad (j, i) \in \mathcal{E}. \tag{2}$$

Particularly, in this article, the physical interpretation of the directed edge $(j, i) \in \mathcal{E}$ is that only agent j can measure the relative bearing of agent i with respect to itself, i.e., $\hat{v}_{ji}$, and not vice versa. As will be highlighted later, we will also assume that only agent 2 is capable of measuring its relative position w.r.t. its neighbor, which is agent 1. Moreover, we assume that the graph $\mathcal{G}$ is triangulated and imposes a hierarchical structure, where agent 1 is the *leader*, agent 2 is the *first follower* with agent 1 acting as its neighbor, agent 3 is the *second follower* following agents 1 and 2, and agents $i \geq 4$ are *ordinary followers* with each one having exactly three neighbors to follow with smaller indices. Hence, we impose the following assumption for constructing $\mathcal{G}$.

Assumption 1: The directed sensing graph $\mathcal{G}$ is constructed such that:

(i) $\mathrm{out}(i) = i - 1, \forall i \leq 3$, and $\mathrm{out}(i) = 3, \forall i \geq 4$;
(ii) if there is an edge between agents i and j, where $i < j$, the direction must be $j \to i$;
(iii) if $(k, i), (k, j) \in \mathcal{E}$ then $(j, i) \in \mathcal{E}$.

Here, $\mathrm{out}(i)$ denotes the out-degree of vertex i that is the number of edges in $\mathcal{E}$ whose source is vertex i and whose sinks are in $\mathcal{V} \backslash \{i\}$. It is important to note that (i) and (ii) of Assumption 1 impose $\mathcal{G}$ to be acyclic minimally persistent with edge set cardinality $|\mathcal{E}| = 3n - 6$ [2]. Moreover, Assumption 1.(iii) ensures that $\mathcal{G}$ is triangulated and composed of acyclic-directed tetrahedrons. Fig. 1(a) shows an example of $\mathcal{G}$ constructed under Assumption 1.

Remark 1: It is known that graphs satisfying Assumption 1 can be systematically constructed using 3D Henneberg type I insertion [19], [21]. Such graphs belong to a class of acyclic minimally persistent graphs, which are the directed counterpart of undirected distance rigid graphs [2], [4], [14]. Minimally persistent graphs (persistent graphs with a minimum number of edges) are favorable in practice since they require a minimum number of relations (sensing) among agents.

Associated with each ordinary follower $l \geq 4$ in $\mathcal{G}$ with three neighbors i, j, and k, we can define a signed volume of the tetrahedron formed by vertices $i < j < k < l$ as follows [21]:

$$\begin{aligned} V_{ijkl} &= \frac{1}{6} \det \begin{bmatrix} 1 & 1 & 1 & 1 \\ p_i & p_j & p_k & p_l \end{bmatrix} \\ &= -\frac{1}{6} (p_i - p_l)^\top [(p_j - p_l) \times (p_k - p_l)]. \end{aligned} \tag{3}$$

The sign of V_{ijkl} is interpreted as follows: If an observer positioned at vertex l observes the sequence of vertices i, j, and k in a counterclockwise orientation with respect to the plane containing i, j, and k, denoted as $\varnothing_{ijk}$, the sign of V_{ijkl} is positive. Conversely, a clockwise observation yields a negative sign for V_{ijkl}. Note that this volume metric becomes zero if any triad of vertices (i.e. i, j, k) becomes collinear or if all four vertices lie on the same plane. We define the stacked signed volumes corresponding to all tetrahedral subgraphs of $\mathcal{G}$ by the mapping $\mathbf{V} : \mathbb{R}^{3n} \to \mathbb{R}^{n-3}$:

$$\mathbf{V}(p) = \left[\ldots, \frac{1}{6} \det \begin{bmatrix} 1 & 1 & 1 & 1 \\ p_i & p_j & p_k & p_l \end{bmatrix}, \ldots \right]^\top, \tag{4}$$

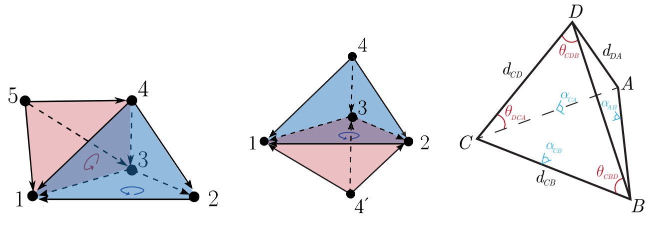

(a) (b) (c)

Fig. 1. (a) A graph constructed under Assumption 1 with 5 agents, which consists of two tetrahedral subgraphs. The blue tetrahedron has a positive volume ($V_{1234} > 0$) and the red one has a negative volume ($V_{1235} < 0$). (b) Position of vertex 4 makes a tetrahedron with positive volume $V_{1234} > 0$ (blue) while its reflected position 4' leads to the same volume ($|V_{1234}| = |V_{1234'}|$) with a negative sign $V_{1234'} < 0$ (red). (c) Tetrahedron $ABCD$ and three of its edge lengths, face angles, and dihedral angles.

$\forall (l,i),(l,j),(l,k) \in \mathcal{E} - \{(2,1),(3,1),(3,2)\}$, where $p = [p_1,\dots,p_n]$ and its m-th ($m \le n-3$) component is the signed volume of the m-th tetrahedron constructed with vertices $i < j < k < l$. For example, the stacked signed volumes of the graph in Fig.1(a) has two elements, where $V_{1234} > 0$ (shown in blue) and $V_{1345} < 0$ (shown in red). It is known that based on the directed sensing graph $\mathcal{G}$ under Assumption 1, we can *uniquely* define a desired formation characterized by the followings [21]:

1) A set of $3n-6$ *desired distances* d^*_{ji}, appointed to the directed edges $(j,i) \in \mathcal{E}$.
2) A set of $n-3$ *desired signed volumes* $V^*_{ijkl} \in \mathbf{V}(p^*)$

Given a desired formation characterized by a graph $\mathcal{G}$ (under Assumption 1) and the corresponding sets of desired distances and signed volumes, the objective is to design a decentralized controller for (1) such that:

$$\|p_i(t) - p_j(t)\| \to d^*_{ji}\ ,\ V_{ijkl}(t) \to V^*_{ijkl} \ \text{ as } \ t \to \infty, \quad (5)$$

for all $(j,i) \in \mathcal{E}$ and all $V_{ijkl} \in \mathbf{V}$, respectively, while avoiding zero distance among all neighboring agents (i.e., $\|p_{ji}\| \neq 0, \forall (j,i) \in \mathcal{E}, \forall t \ge 0$).

Note that characterization of the desired formation just by a set of desired distances is not unique and suffers from local shape convergence and reflection issues due to the existence of undesired shapes (namely reflection, flip, and flex ambiguities) (see [2], [16], [18] for examples). To tackle these issues, extra types of formation parameters (e.g., signed volume, signed area, edge-angle) have been recently employed along with the distances to characterize the desired formation uniquely, which is necessary for having global shape convergence [15], [17], [18], [21]. Particularly, the notion of strong congruency was introduced in [20] and [21] for distinguishing the desired shape of a formation from its reflected version. It is known that satisfaction of (5) is equivalent to strong congruency [21] between the actual formation of the agents and the desired formation (see [21], Lemma 1]). This means that if (5) gets satisfied, the agents can achieve the desired formation only up to rotations and translations [21]. As an example, consider distances $\|p_{41}\|, \|p_{42}\|, \|p_{43}\|$, and the signed volume V_{1234} in Fig. 1(b), where $V_{1234} > 0$. Assuming vertex $4'$ as the reflected version of vertex 4 without altering its distances with respect to 1, 2 and 3, then we get $V_{1234'} < 0$. In general, this property allows us to distinguish the position of agent l from its reflection with respect to the plane passing through agents i, j, and k.

III. Bispherical Coordinate System

Consider a tetrahedron defined by vertices A,B,C,D. It encompasses 4 *faces* $F_{\mathcal{PQR}}$ for each triad of $\{\mathcal{P},\mathcal{Q},\mathcal{R}\} \in \{A,B,C,D\}$, 6 *edge lengths* $d_{\mathcal{PQ}}$ for each unique pair of vertices $\{\mathcal{P},\mathcal{Q}\} \in \{A,B,C,D\}$, 12 *face angles* $\theta_{\mathcal{PQR}}$ defined by the angles between edges $\mathcal{PQ}$ and $\mathcal{QR}$ for each set of vertices $\{\mathcal{P},\mathcal{Q},\mathcal{R}\} \in \{A,B,C,D\}$, and 6 *dihedral angles* $\alpha_{\mathcal{PQ}}$ representing the angles between the faces adjoining edge $\mathcal{PQ}$ for each vertex pair $\{\mathcal{P},\mathcal{Q}\} \in \{A,B,C,D\}$. Fig.1(c) illustrates three of the edge lengths, face angles, and dihedral angles on tetrahedron $ABCD$.

A. Bispherical Coordinates

Now, consider a tetrahedral subgraph of $\mathcal{G}$ where $i < j < k < l$. The first bispherical coordinate, denoted by $\xi_l \in [0,\pi]$, is equal to the edge angle θ_{ilj}, which can be expressed as the angle between relative bearing vectors from agent l to the neighboring agents i and j as follows:

$$\xi_l := \theta_{ilj} = \cos^{-1}\left(\hat{v}_{li}^\top \hat{v}_{lj}\right), \quad l \in \mathcal{V}\backslash\{1,2,3\}. \quad (6)$$

Note that for agent 3 we define: $\xi_3 := \cos^{-1}\left(\hat{v}_{31}^\top \hat{v}_{32}\right)$. Fig. 2(a) illustrates the relative bearing vectors among the agents in a tetrahedral subgraph and the first bispherical coordinate ξ_k and ξ_l for agents k and l, respectively. Defining the *ratios of distances* $r_{lij} := \|p_{li}\| / \|p_{lj}\| = d_{li}/d_{lj}$ and $r_{lik} := \|p_{li}\| / \|p_{lk}\| = d_{li}/d_{lk}$ for $l \in \mathcal{V}\backslash\{1,2,3\}$, one can define the second bispherical coordinate η_l as:

$$\eta_l := \ln r_{lij} = \ln \frac{\|p_{li}\|}{\|p_{lj}\|}, \quad l \in \mathcal{V}\backslash\{1,2,3\}, \quad (7)$$

where $\eta_l \in \mathbb{R}$. Note that, when agent l approaches agent i or agent j (i.e., either $d_{li} \to 0$ or $d_{li} \to 0$), η_l tends to $\pm\infty$. Note that, only one ratio of the distance is defined for agent 3, that is $\eta_3 = \ln(d_{31}/d_{32})$. Finally, the third bispherical coordinate, denoted by $\varphi_l \in [0, 2\pi)$, $l \ge 4$, is the angle between half-planes $\varlozenge_{ijk}$ and $\varlozenge_{ijl}$ measured in the counterclockwise direction from the former to the latter (see Fig. 2(b)). In particular, one can obtain φ_l as follows:

$$\varphi_l = \begin{cases} \alpha_{ij} & \text{if } \operatorname{sgn}\left(\hat{v}_{li}^\top \left(\hat{v}_{lj} \times \hat{v}_{lk}\right)\right) = \operatorname{sgn}\left(V_{ijkl}\right) > 0 \\ 2\pi - \alpha_{ij} & \text{if } \operatorname{sgn}\left(\hat{v}_{li}^\top \left(\hat{v}_{lj} \times \hat{v}_{lk}\right)\right) = \operatorname{sgn}\left(V_{ijkl}\right) < 0 \\ \pi & \text{if } V_{ijkl} = 0 \text{ and } \left(\hat{v}_{ji} \times \hat{v}_{li}\right)^\top \left(\hat{v}_{ji} \times \hat{v}_{ki}\right) < 0 \\ 0 & \text{otherwise} \end{cases}, \quad (8)$$

where $\alpha_{ij} \in (0,\pi)$ is the dihedral angle of the tetrahedron $ijkl$ on edge (j,i). Note that the sign of $\hat{v}_{li}^\top \left(\hat{v}_{lj} \times \hat{v}_{lk}\right)$ is the same as the sign of V_{ijkl} since $\hat{v}_{li}^\top \left(\hat{v}_{lj} \times \hat{v}_{lk}\right)$ consists of the normalized vectors used in (3). The third and fourth cases in (8) correspond to when agent l and all its neighbors are in the same plane meaning that $V_{ijkl} = 0$. As α_{ij} is undefined in these cases, if the half-plane including agents i, j, and k is the same half-plane including agents i, j, and l then $\varphi_l = 0$. Otherwise, $\varphi_l = \pi$. Moreover, when 3 or 4 number of agents in the subgraph with agents i, j, k, and l

are collinear, $\varphi_l = 0$. Finally, note that for agent 3 we always have $\varphi_3 = 0$ since it always lies on $\varDelta_{123}$. Also, note that one can find $\beta_{ij} := \cos \alpha_{ij}$ by calculating the angle between the normal vectors of faces F_{ijk} and F_{ijl} as follows:

$$\beta_{ij} = \frac{(\hat{v}_{ij} \times \hat{v}_{ik})^\top (\hat{v}_{ij} \times \hat{v}_{il})}{\|\hat{v}_{ij} \times \hat{v}_{ik}\| \|\hat{v}_{ij} \times \hat{v}_{il}\|} = \frac{\cos\theta_{kil} - \cos\theta_{jik}\cos\theta_{jil}}{\sin\theta_{jik}\sin\theta_{jil}}. \tag{9}$$

B. Desired Formation Characterization

Given a target formation, one can use the desired bispherical coordinates of agent $m \geq 3$ with respect to its neighbors to uniquely characterize the desired formation shape using the following expressions:

$$\eta_l^* = \ln \frac{d_{li}^*}{d_{lj}^*}, \quad \xi_l^* = \theta_{ilj}^* = \cos^{-1}\left(\frac{{d_{li}^*}^2 + {d_{lj}^*}^2 - {d_{ji}^*}^2}{2 d_{li}^* d_{lj}^*}\right)$$
$$\varphi_l^* = \begin{cases} \alpha_{ij}^* = \cos^{-1}\left(\frac{\cos\theta_{kil}^* - \cos\theta_{jik}^*\cos\theta_{jil}^*}{\sin\theta_{jik}^*\sin\theta_{jil}^*}\right) & \text{if } V_{ijkl}^* > 0 \\ 2\pi - \alpha_{ij}^* & \text{if } V_{ijkl}^* < 0 \end{cases} \tag{10}$$

Note that, for agent 3 we have $\eta_3^* := \ln \frac{d_{31}^*}{d_{32}^*}$ and $\xi_3^* := \cos^{-1}\left(\frac{{d_{31}^*}^2 + {d_{32}^*}^2 - {d_{21}^*}^2}{2 d_{31}^* d_{32}^*}\right)$.

Lemma 1: Given a desired formation shape based on a specific directed sensing graph $\mathcal{G} = (\mathcal{V}, \mathcal{E})$ under Assumption 1, satisfying

$$\|p_2(t) - p_1(t)\| \to d_{21}^*, \qquad \text{as } t \to \infty \tag{11a}$$
$$\xi_m(t) \to \xi_m^*\ ,\ \eta_m(t) \to \eta_m^*, \quad m \geq 3, \quad \text{as } t \to \infty \tag{11b}$$
$$\varphi_m(t) \to \varphi_m^*, \quad m \geq 4, \quad \text{as } t \to \infty \tag{11c}$$

is equivalent to the satisfaction of (5).

Proof: The proof has been omitted due to lack of space and can be found in [22]. ■

Recall that based on (5), only the first follower (agent 2) and second follower (agent 3) have to keep specific distances with respect to their neighbors, while all other agents (ordinary followers) must preserve a designated signed volume and three exact distances relative to their neighboring agents. Thus, to achieve the target formation through satisfying (5), each ordinary follower ($m \geq 4$) is required to control four variables: three distances and a signed volume. Nevertheless, introducing an additional shape constraint (i.e. signed volume) for the ordinary followers may cause new undesirable equilibria due to the interaction of distance and signed-volume constraints at particular agent locations (refer to [15], [16], [17], [18] for an in-depth discussion and examples in 2D formations). It is crucial to note that these four variables do not always form an orthogonal space, in which each one can be controlled independently via moving along orthogonal directions. Lemma 1 circumvents this by requiring ordinary followers to control merely three orthogonal (independent) formation variables (11b) and (11c). We will exploit this property to design decentralized formation controllers for the follower agents, as detailed in Section IV, thereby allowing (almost) global convergence to the desired shape. Moreover, as mentioned earlier, by altering the distance between agents 2 and 1, $\|p_2(t) - p_1(t)\|$, the formation's scale at steady-state can be controlled. Here, scaling refers to maintaining all angles while adjusting all edge lengths proportionally. Thus, by dynamically setting a target distance $d_{21}^*(t)$ relative to the leader, the first follower can modulate the formation's scale, which is vital in real-world formation control scenarios like navigating through tight spaces or avoiding obstacles.

C. Bispherical Coordinates Basis Vectors

In the previous subsections we showed that the desired positions of agents $l \geq 4$ w.r.t. their neighbors can be uniquely characterized by bispherical coordinates. Here, we derive the bispherical coordinate basis associated with each follower agent $l \geq 4$.

Note that, in each tetrahedral subgraph of $\mathcal{G}$, where $i < j < k < l,\ l \geq 4$, one can define a virtual local Cartesian coordinate frame for agent l denoted by $\{C_l\}$, with its origin located in the middle of the $i - j$ line (see Fig. 2(a)). The basis of $\{C_l\}$ can be written in terms of the relative bearing vectors (expressed in a global coordinate frame) associated with agent l as follows:

$$\hat{X}_l = -\hat{v}_{ji}, \quad \hat{Z}_l = \frac{\hat{v}_{ji} \times \hat{v}_{ki}}{\|\hat{v}_{ji} \times \hat{v}_{ki}\|}, \quad \hat{Y}_l = \hat{Z}_l \times \hat{X}_l. \tag{12}$$

The bispherical coordinates are related to the $\{C_l\}$ frame with the following (almost) one-to-one (except at the foci of the bispherical coordinates, i and j) transformation [23]:

$$x_l^{[C_l]} = \frac{a_l \sinh\eta_l}{\cosh\eta_l - \cos\xi_l},\ y_l^{[C_l]} = \frac{a_l \sin\xi_l \cos\varphi_l}{\cosh\eta_l - \cos\xi_l},\ z_l^{[C_l]} = \frac{a \sin\xi_l \sin\varphi_l}{\cosh\eta_l - \cos\xi_l}, \tag{13}$$

where $p_l^{[C_l]} = [x_l^{[C_l]}, y_l^{[C_l]}, z_l^{[C_l]}]^\top \in \mathbb{R}^3$ is the position of vertex l with respect to frame $\{C_l\}$ and $a_l := 0.5\,\|p_{ji}\| > 0$. The bispherical coordinate system $(\xi_l, \eta_l, \varphi_l)$ is indeed a 3D orthogonal curvilinear coordinate system [23], [24] (similar to the spherical coordinate system), thus, a local orthogonal basis can be defined at each point in the 3D plane of $\{C_l\}$ showing the directions of increase for ξ_l, η_l, and φ_l. Figs. 2 and 3 altogether show orthogonal bispherical coordinates basis $\hat{\xi}_l$, $\hat{\eta}_l$, and $\hat{\varphi}_l \in \mathbb{R}^3$ associated with $\{C_l\}$ at some arbitrary points of interest.

Remark 2: The relations in (12) and (13) are still valid for agent 3. Indeed since agent 3 is always on $\varDelta_{123}$ plane, we have $z_3^{[C_l]} = 0$ and $\varphi_3 = 0$. Moreover, when agents i, j, and k are collinear or collocated, the basis in 12 are not well-defined. To tackle this issue, we can use Algorithm 1 of [21], which guarantees that $\hat{v}_{ji} \times \hat{v}_{ki}$ is well defined. This means that the output vector of [21, Algorithm 1] will be an arbitrarily selected vector perpendicular to p_{ji} and p_{ki} when agents are collinear or collocated. Also, it is worth mentioning that the unit orthogonal basis of $\{C_l\}$ are the normalized version of the orthogonal basis defined in [21].

Lemma 2: For a given tetrahedral directed sub-graph as in Fig. 2(a), the bispherical coordinates basis $\hat{\xi}_l, \hat{\eta}_l, \hat{\varphi}_l,\ l \geq 4$ (see Figs. 3 and 2) associated with the virtual local Cartesian frame $\{C_l\}$, $l \geq 4$ in Fig. 2 can be expressed with respect to $\{C_l\}$ as follows: $\hat{\xi}_l = f_1\hat{X}_l + f_2 f_3 \hat{Y}_l + f_2 f_4 \hat{Z}_l,\ \hat{\eta}_l = -f_2\hat{X}_l + f_1 f_3 \hat{Y}_l + f_1 f_4 \hat{Z}_l,\ \hat{\varphi}_l = -f_4\hat{Y}_l + f_3\hat{Z}_l$, where $\hat{X}_l$, $\hat{Y}_l$, and $\hat{Z}_l$ are given by (12), which are the Cartesian basis vectors assigned to agent l in $\{C_l\}$ and $f_1(\xi_l, \eta_l, \varphi_l) = \frac{-\sinh\eta_l \sin\xi_l}{\cosh\eta_l - \cos\xi_l}$, $f_2(\xi_l, \eta_l, \varphi_l) = \frac{\cosh\eta_l\cos\xi_l - 1}{\cosh\eta_l - \cos\xi_l}$, $f_3(\varphi_l) =$

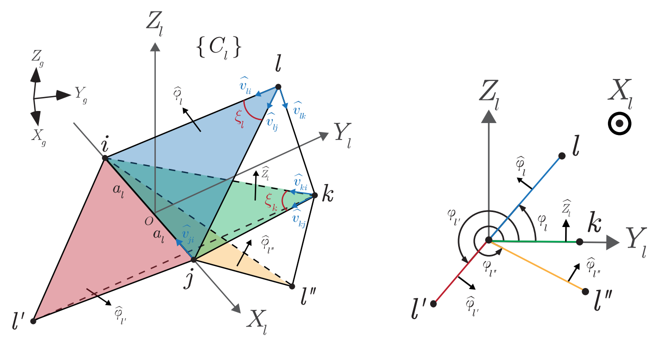

(a) (b)

Fig. 2. (a) Showing direction of $\hat{\varphi}$ for for three cases of agent l positions (indicated by l, l' and l''). Note that agents i, j, l, and l' are on the same plane but different half-planes leading to opposite $\hat{\varphi}$ directions. (b) 2D view of $\{C_l\}$ showing $\hat{\varphi}$ and φ for some different positions of agent l. (indicated by l, l' and l'')

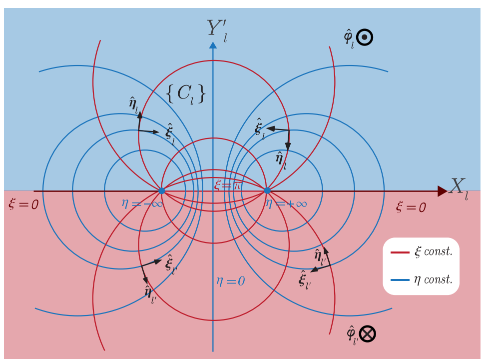

Fig. 3. 2D view of $i-j-l$ plane in Fig. 2(a). In the entire upper half plane (blue) $\hat{\varphi}$ is pointing outwards, while it points inwards in the lower half plane (red). Y_l' is rotated version of Y_l around X_l lying down in $i-j-l$ plane. This figure depicts the projection of the isoquant surfaces of ξ, η on $i-j-l$ plane and their corresponding orthogonal basis vectors $\hat{\xi}$ and $\hat{\eta}$ for two different positions of l and l'. Note that $\hat{\xi}$ and $\hat{\eta}$ always lie on the $i-j-l$ plane, which are perpendicular to $\hat{\varphi}$.

$\cos\varphi_l,\ f_4(\varphi_l)=\sin\varphi_l$. Note that $\varphi_3=0$, and $\hat{\varphi}_3=\hat{Z}_3$ for agent 3.

Proof: The proof is simple and can be followed similarly to [23]. ■

IV. Proposed Controller

A. Formation Errors

To quantify the control objectives we define 4 types of error variables. First, *squared distance error* between agents 2 and 1 is defined as:

$$e_d=\|p_{21}\|^2-d_{21}^{*2}. \tag{14}$$

Second, the *edge-angle* and *logarithmic ratio of the distances errors* are defined as:

$$e_{\xi_m}=\xi_m-\xi_m^*,\quad e_{\eta_m}=\eta_m-\eta_m^*,\quad m\geq 3, \tag{15}$$

where ξ_m^*, and η_m^* are given in (10). Finally, the *dihedral angle error* is defined as:

$$e_{\varphi_m}=\varphi_m-\varphi_m^*,\quad m\geq 4, \tag{16}$$

where φ_l^* is given in (10). Note that (15) and (16) are independent (orthogonal) error variables defined only for the followers. More precisely, by moving along each bispherical coordinate's basis, $\hat{\xi}_m$, $\hat{\eta}_m$, and $\hat{\varphi}_m$, each follower can reduce (15) and (16) respectively, without affecting the other error variable. Finally, due to the above discussion and Lemma 1, by adopting the bispherical coordinates approach, the control objective of (5) is met by zero stabilization of the error signals defined in (14), (15), and (16).

B. Proposed Control Law and Stability Analysis

Notice that in the proposed formation control setup, the leader (agent 1) does not participate in forming the desired shape, thus its behavior is independent of the other agents. In this respect, the leader's control law is $u_1=0$ without loss of generality. We propose the following formation control laws:

$$u_2=\kappa_2 e_d p_{21}=\kappa_2 e_d\|p_{21}\|\,\hat{v}_{21}, \tag{17a}$$

$$u_3=-\kappa_3 e_{\xi_3}\hat{\xi}_3-\lambda_3 e_{\eta_3}\hat{\eta}_3, \tag{17b}$$

$$u_l=-\kappa_l e_{\xi_l}\hat{\xi}_l-\lambda_l e_{\eta_l}\hat{\eta}_l-\gamma_l e_{\varphi_l}\hat{\varphi}_l,\quad l\geq 4, \tag{17c}$$

where κ_2, κ_3, λ_3, and $\kappa_l,\lambda_l,\gamma_l$, $l\geq 4$, are positive control gains and $\hat{\xi}_l$, $\hat{\eta}_l$, and $\hat{\varphi}_l$ are the bispherical coordinates basis associated with ordinary followers. Note that the proposed control laws in (17) are decentralized, since each agent only uses the measured information w.r.t. its neighbors and can obtain all the required info via its local sensing. (see [22].) Note that although the proposed control laws (17) are given with respect to a virtual coordinate frame $\{C_l\}$, $l\geq 3$ we emphasize that the proposed formation controller can be implemented in any arbitrarily oriented local coordinate frame. Refer to [22] for more details.

Theorem 1: Consider a group of n agents with dynamics (1) in a 3D space. Let the desired formation be defined by a directed graph $\mathcal{G}=(\mathcal{V},\mathcal{E})$ under Assumption 1 along with the sets of desired formation parameters d_{21}^*, ξ_m^*, η_m^*, $m\geq 3$, and φ_m^*, $m\geq 4$. The decentralized control protocol (17) ensures $\|p_{ji}\|\neq 0,\forall(j,i)\in\mathcal{E},\forall t\geq 0$, and renders the formation errors in (15) and (16) almost globally asymptotically stable, which gurantees the satisfaction of the desired objectives in (11).

Proof: The proof has been omitted due to lack of space and can be found in [22]. ■

V. Simulation Results

Consider six agents that are distributed at random positions (leader is in origo.) in a 3D workspace at $t=0$. The objective is to form a unit octahedron until $t=10$ seconds and then double up its scale until $t=20$ seconds under control law (17). The edge set of the directed sensing graph (obeying Assumption 1) is considered as $\mathcal{E}=\{(2,1),(3,1),(3,2),(4,1),(4,2),(4,3),(5,2),(5,3),(5,4),(6,3),(6,4),(6,5)\}$. The sensing graph among the agents is depicted in 5(a). The desired shape is characterized by setting all of the desired lengths in the edge set equal to 1 except for $d_{32}^*=d_{64}^*=\frac{\sqrt{2}}{2}$. The desired signed volumes are assumed to be $V_{1234}^*=V_{2345}^*=-V_{3456}^*=\frac{\sqrt{2}}{12}$. To realize the formation scaling the desired distance between agents 1

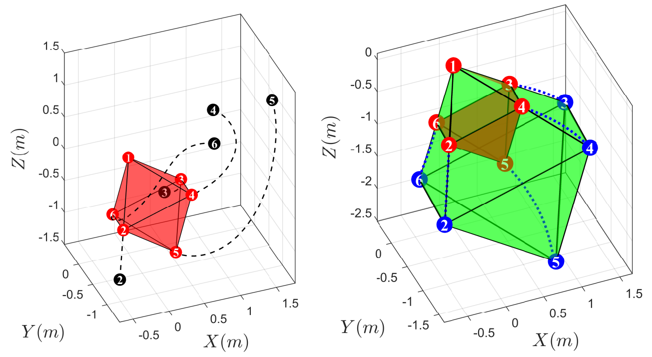

(a) (b)

Fig. 4. (a) Trajectory of agents until $t = 10$. (b) Scaling simulation: agents scaling up after $t = 10$ because of a change in d_{21}^*.

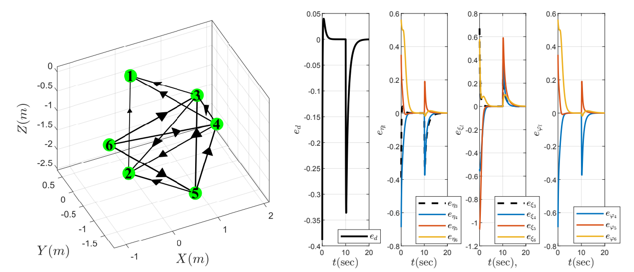

(a) (b)

Fig. 5. (a) Sensing graph among agents. (b) Formation errors vs time.

and 2 is initially set to $d_{21}^* = 1$ until $t = 10$ and then it is changed to $d_{21}^* = 2$. The control gains in (17a),(17b), and (17c) are all set to 2. The trajectory of each agent during $t \in [0, 10]$, where the desired formation scale is equal to 1 is shown in Fig. 4(a). Fig. 4(b) shows the final scaled-up shape as well as the trajectories of the agents during $t \in [10, 20]$.

The evolution of squared distance error and bispherical formation errors, defined in (14), (15), and (16), are shown in Fig. 5(b). The results show that the agents successfully converge to the desired formation after approximately 10 units of time despite their random initial positions. Moreover, after the step shift in agent 2's desired distance at $t = 10s$, which induces a sudden increase in the follower's formation errors (see Fig. 5(b)), the formation eventually scales up as soon as the follower's formation errors converge back to zero.

VI. Conclusion

We introduced a novel 3D formation control scheme, with (almost) global convergence to the desired shape under acyclic triangulated directed sensing topologies. We utilized orthogonal bispherical coordinates to uniquely characterize the desired formation shape and effectively avoid undesired equilibria imposed by the controller design. Our proposed control scheme also allows for formation scaling through adjustments of the distance between agents 1 and 2. Applying the stability theory of cascade-connected systems, we established that the proposed decentralized controllers make the closed-loop system almost globally asymptotically stable. Furthermore, we reasoned that the proposed control scheme can be readily implemented in arbitrarily oriented local coordinate frames of the (follower) agents using onboard vision sensors.

References

[1] K.-K. Oh, M.-C. Park, and H.-S. Ahn, "A survey of multi-agent formation control," *Automatica*, vol. 53, pp. 424–440, 2015.

[2] B. D. Anderson, C. Yu, B. Fidan, and J. M. Hendrickx, "Rigid graph control architectures for autonomous formations," *IEEE Control Systems Magazine*, vol. 28, no. 6, pp. 48–63, 2008.

[3] F. Mehdifar, C. P. Bechlioulis, F. Hashemzadeh, and M. Baradarannia, "Prescribed performance distance-based formation control of multi-agent systems," *Automatica*, vol. 119, p. 109086, 2020.

[4] T. H. Summers, C. Yu, B. D. Anderson, and S. Dasgupta, "Control of minimally persistent leader-remote-follower formations in the plane," in *2009 European Control Conference (ECC)*.

[5] S. Zhao and D. Zelazo, "Bearing rigidity and almost global bearing-only formation stabilization," *IEEE Transactions on Automatic Control*, vol. 61, no. 5, pp. 1255–1268, 2015.

[6] G. Jing, G. Zhang, H. W. J. Lee, and L. Wang, "Angle-based shape determination theory of planar graphs with application to formation stabilization," *Automatica*, vol. 105, pp. 117–129, 2019.

[7] L. Chen and M. Cao, "Angle rigidity for multi-agent formations in 3d," *IEEE Transactions on Automatic Control*, 2023.

[8] L. Chen and Z. Sun, "Globally stabilizing triangularly angle rigid formations," *IEEE Transactions on Automatic Control*, vol. 68, no. 2, pp. 1169–1175, 2022.

[9] K. Cao, Z. Han, X. Li, and L. Xie, "Ratio-of-distance rigidity theory with application to similar formation control," *IEEE Transactions on Automatic Control*, vol. 65, no. 6, pp. 2598–2611, 2019.

[10] S.-H. Kwon, Z. Sun, B. D. Anderson, and H.-S. Ahn, "Sign rigidity theory and application to formation specification control," *Automatica*, vol. 141, p. 110291, 2022.

[11] F. Mehdifar, C. P. Bechlioulis, J. M. Hendrickx, and D. V. Dimarogonas, "2-d directed formation control based on bipolar coordinates," *IEEE Transactions on Automatic Control*, 2022.

[12] R. Tron, J. Thomas, G. Loianno, K. Daniilidis, and V. Kumar, "A distributed optimization framework for localization and formation control: Applications to vision-based measurements," *IEEE Control Systems Magazine*, vol. 36, no. 4, pp. 22–44, 2016.

[13] S. Mou, M.-A. Belabbas, A. S. Morse, Z. Sun, and B. D. Anderson, "Undirected rigid formations are problematic," *IEEE Transactions on Automatic Control*, vol. 61, no. 10, pp. 2821–2836, 2015.

[14] C. Yu, J. M. Hendrickx, B. Fidan, B. D. Anderson, and V. D. Blondel, "Three and higher dimensional autonomous formations: Rigidity, persistence and structural persistence," *Automatica*, vol. 43, no. 3, pp. 387–402, 2007.

[15] T. Sugie, F. Tong, B. D. Anderson, and Z. Sun, "On global convergence of area-constrained formations of hierarchical multi-agent systems," in *2020 59th IEEE Conference on Decision and Control (CDC)*.

[16] T. Liu, M. de Queiroz, P. Zhang, and M. Khaledyan, "Directed formation control of n planar agents with distance and area constraints," in *2019 American Control Conference (ACC)*.

[17] Y. Cao, Z. Sun, B. D. Anderson, and T. Sugie, "Almost global convergence for distance-and area-constrained hierarchical formations without reflection," in *2019 IEEE 15th International Conference on Control and Automation (ICCA)*.

[18] B. D. Anderson, Z. Sun, T. Sugie, S.-i. Azuma, and K. Sakurama, "Formation shape control with distance and area constraints," *IFAC Journal of Systems and Control*, vol. 1, pp. 2–12, 2017.

[19] R. Babazadeh and R. R. Selmic, "Directed distance-based formation control of nonlinear heterogeneous agents in 3-d space," *IEEE Transactions on Aerospace and Electronic Systems*, 2022.

[20] T. Liu, M. de Queiroz, and F. Sahebsara, "Distance-based planar formation control using orthogonal variables," in *2020 IEEE Conference on Control Technology and Applications (CCTA)*.

[21] T. Liu and M. de Queiroz, "An orthogonal basis approach to formation shape control," *Automatica*, vol. 129, p. 109619, 2021.

[22] O. Mirzaeedodangeh, F. Mehdifar, and D. V. Dimarogonas, "3d directed formation control with global shape convergence using bispherical coordinates," *arXiv preprint arXiv:2403.13609*, 2024.

[23] G. B. Arfken, *Mathematical methods for physicists. 2nd ed.* Academic Press, 1970.

[24] P. Moon and D. E. Spencer, *Field theory handbook incl. coordinate systems, differential equations, and their solutions*. Springer, 1988.